TITLE PAGE

Citation Format:

A. Behera, L. Di Sieno, A. Pifferi, F. Martelli, A. Dalla Mora, "Study of optimal measurement conditions for time-domain diffuse optics systems," in Biophotonics: Photonic Solutions for Better Health Care VI, Jürgen Popp, Valery V. Tuchin and Francesco Saverio Pavone ed., Vol 10685 of Proceedings of SPIE (SPIE, Bellingham, WA, 2018), paper 1068514.

Copyright notice:

DOI abstract link:

https://doi.org/10.1117/12.2307370

Study of optimal measurement conditions for time-domain diffuse optics systems

Anurag Behera, Laura Di Sieno, Antonio Pifferi, Fabrizio Martelli, Alberto Dalla Mora

Anurag Behera, Laura Di Sieno, Antonio Pifferi, Fabrizio Martelli, Alberto Dalla Mora, "Study of optimal measurement conditions for time-domain diffuse optics systems," Proc. SPIE 10685, Biophotonics: Photonic Solutions for Better Health Care VI, 1068514 (17 May 2018); doi: 10.1117/12.2307370

SPIE.

Event: SPIE Photonics Europe, 2018, Strasbourg, France

Study of optimal measurement conditions for time-domain diffuse optics systems

Anurag Behera[a*], Laura Di Sieno[a], Antonio Pifferi[a,b] , Fabrizio Martelli[c] and Alberto Dalla Mora[a]
[a] Politecnico di Milano, Dipartimento di Fisica, Piazza Leonardo da Vinci 32, 20133 Milano, Italy
[b] Consiglio Nazionale delle Ricerche, Istituto di Fotonica e Nanotecnologie, Piazza Leonardo da Vinci 32, 20133 Milano, Italy
[c] Università degli Studi di Firenze, Dipartimento di Fisica e Astronomia, Via G. Sansone 1, 50019 Sesto Fiorentino, Firenze, Italy

ABSTRACT

Light is a powerful non-invasive tool that can be exploited to probe highly scattering media like biological tissues for different purposes, from the detection of brain activity to the characterization of cancer lesions. In the last decade, time-domain diffuse optics (TDDO) systems demonstrated improved sensitivity when using time-gated acquisition chains and short source-detector separations (ρ), both theoretically and experimentally. However, the sensitivity to localized absorption changes buried inside a diffusive medium strongly depends on many parameters such as: SDS, laser power, delay and width of the gating window, absorption and scattering properties of the medium, instrument response function (IRF) shape, etc. In particular, relevant effects due to slow tails in the IRF were noticed, with detrimental effects on performances. We present simulated experimental results based on the diffusion approximation of the Radiative Transfer Equation and the perturbation theory subjected to the Born approximation. To quantify the system sensitivity to deep (few cm) and localized absorption perturbations, we exploited contrast and contrast-to-noise ratio (CNR), which are internationally agreed on standardized figures of merit. The purpose of this study is to determine which parameters have the greatest impact on these figures of merit, thus also providing a range of best operative conditions. The study is composed by two main stages: the former is a comparison between simulations and measurements on tissue-mimicking phantom, while the latter is a broad simulation study in which all relevant parameters are tuned to determine optimal measurement conditions. This study essentially demonstrates that under the influence of the slow tails in the IRF, the use of a small SDS no longer corresponds to optimal contrast and CNR. This work sets the ground for future studies with next-generation of TDDO components, presently under development, providing useful hints on relevant features to which one should take care when designing TDDO components.
Keywords: time-domain optical imaging; diffusive media; single-photon detector; medical imaging; simulations

1. INTRODUCTION

Diffuse optics allows us to non-invasively probe highly scattering media [1] like biological tissues [2] for various purposes, from the detection of brain activity[3] to the characterization of cancer lesions [4] and to the tomography application[5]. Time-domain (TD) diffuse optics systems, in particular, have shown immense potential [6]and in the last decade or so, have demonstrated an improved sensitivity when using time-gated acquisition chains and short source-detector separations (SDS), both theoretically as well as experimentally[7][8]

.

TD approach involves the injection of fast light pulses into the medium and collection of the photons that diffuse through the medium and are reemitted at a certain distance from the source, as the distribution of time of flights (DTOF) of the photons. The background absorption - μ_a - and reduced background scattering - μ'_s- properties result from different physical processes and hence, they affect the DTOF differently and can be extracted independently.

However, the sensitivity to localized absorption changes buried inside a diffusive medium strongly depend on the system parameters such as: laser power, instrument response function (IRF) shape [9], responsivity (i.e. efficiency in light harvesting) of the system, as well as the optical and geometric parameters such as absorption and scattering coefficients of the medium, perturbation size etc.

Biophotonics: Photonic Solutions for Better Health Care VI, edited by Jürgen Popp, Valery V. Tuchin, Francesco Saverio Pavone, Proc. of SPIE Vol. 10685, 1068514

In particular, relevant effects due to slow tails in the IRF[10] were noticed, with detrimental effects on performances.

Here we present a simulation study based on the Radiative Transfer Equation under diffusion approximation, using perturbation theory under Born approximation. To quantify the system's sensitivity to deep (few cm) and localized absorption perturbations, we exploited contrast and contrast-to-noise ratio (CNR), which are suitable standardized figures of merit internationally agreed among different research institutions (defined in the nEUROPt protocol)[11]. The dual goal of this study is: i) to provide a guide to scientists to choose the best conditions for measurements protocols and ii) to understand which parameters are critical for the performance of the system, to enable further technological developments. The study consists of two stages. First, is a comparative study of the Contrast and CNR between simulations and measurements on tissue-mimicking phantoms. Second, a broad study to obtain an insight into the interplay of various parameters and their effect on the system performance. The paper is organized as follows: in Sec. 2 we describe the experimental setup, the simulation tool, and the data analysis; Sec. 3 deals with the results obtained phantom measurements and simulations; finally, in Sec. 4 we draw the conclusions of the work.

2. MATERIALS AND METHODS

2.1.1 Experiment

A four-wave mixing laser at 820 nm wavelength featuring pulses of duration < 100 ps at 40 MHz repetition rate and 90 mW average power was used for providing light pulses. After adequate attenuation by means of a stack of variable optical attenuators, light was then coupled into 50 μm core diameter fiber through a collimator and sent into the medium. The maximum average power of about 50 mW was used on the surface. A 200 μm core diameter fiber was used to collect the photons exiting the medium at a variable ρ, which were then focused onto the detector (fast-gated SPAD, with an active area of 100 μm diameter). An output voltage pulse is generated by the detector every time a photon impinges on its surface. This signal was then fed to the "start" input of the Time-Correlated Single-Photon Counting (TCSPC) board (SPC 130, Becker and Hickl GmbH, Germany). On the other hand, the signal given by the laser and synchronous to the light pulse ("sync") was split in two. One half was sent to the "stop" input of the TCSPC. Since the SPAD is normally OFF, the other half was used as triggering signal to the fast-gated SPAD ("hardware gate" in Fig.1), thus switching ON the detector in about 200 ps in order to enable the detection of photons. An electric gate width of 5 ns was set. The opening of the electric gate was changed by delaying the triggering signal through a home-made transmission-line based delayer (minimum step: 25 ps) . Following the procedure described in the nEUROPt protocol, the optical perturbation was immersed in the liquid medium in an upright position with the help of a rigid wire which was inserted from underneath.

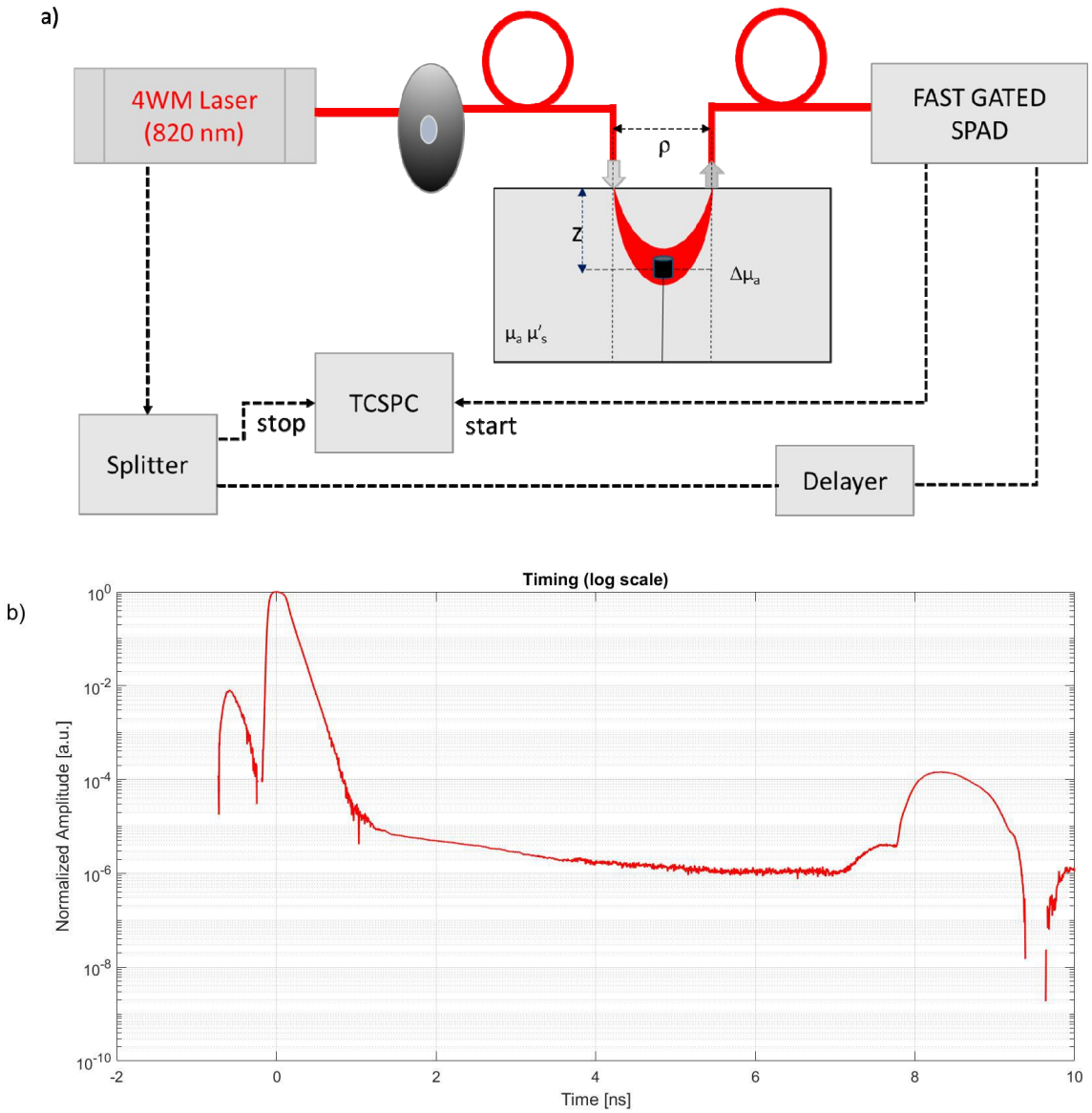

Figure 1. (a) Schematics of the experimental setup used for measurements (dashed line: electrical connections; solid lines: optical path and (b) reconstructed IRF of the setup.

To provide the scattering and absorption properties a liquid phantom based on a 20% solution of Intralipid and Higgins Indian ink was used [12]. 5 phantoms were fabricated to span a wide range of absorption and scattering values. i) $\mu_a = 0.05$ cm^{-1} and $\mu_s' = 10$ cm^{-1}; ii) $\mu_a = 0.1$ cm^{-1} and $\mu_s' = 10$ cm^{-1}; iii) $\mu_a = 0.1$ cm^{-1} and $\mu_s' = 5$ cm^{-1} iv) $\mu_a = 0.1$ cm^{-1} and $\mu_s' = 15$ cm^{-1}; v) $\mu_a = 0.2$ cm^{-1} and $\mu_s' = 10$ cm^{-1}. A totally absorbing black PVC cylinder (height equal to diameter) of volumes 25, 50, 100, 250, 500 mm^3 which for a medium with $\mu_s' = 10$ cm^{-1}, corresponds to $\Delta\mu_a$ values of 0.065, 0.100, 0.162, 0.362, 0.952 cm^{-1} respectively[13], was suspended in the solution and moved along the z direction.

For a given set of background optical properties, measurements at various ρ (2, 4, 6, 8, 10, 15, 20, 25 and 30 mm) values were carried. Having set the ρ, the perturbation was aligned half way between the injection and collection fibers. The depth of inclusion (z) was taken as the distance from the surface of the phantom to the center of cylinder height. The depth was varied from 5 to 30 mm in steps of 2.5 mm using a motorized axis. 8 different sections of the DTOF curves were acquired for 5 repetitions of 1 s, at each depth by changing the delay of the signal that generates the 5 ns hardware

gate window. The repetitions were summed up to increase the signal to noise ratio. The 'standard' background phantom (μ_a= 0.1 cm^{-1} and μ_s'= 10 cm^{-1}) was used to study the effect of absorption perturbation. While, a 100 mm^3 black volume was used to study the effect of a change in background optical properties.

2.2 Simulations

The simulation is based on the diffusion approximation of the Radiative Transport Equation under the Extrapolated Boundary conditions and Born approximation [14] In order to take into account, the non-idealities of the real system the theoretical DTOF was convoluted with different IRFs. The maximum number of counts per DTOF was limited to 10^6 counts/s to take into account the finite count rate of the system. The huge influx of early photons, especially at short ρ, was suppressed by slicing the DTOF before applying the count rate limitations. The system responsivity of the system – as defined in the BIP Protocol [8]- was used to realistically estimate the DTOF amplitude– converting the reflectance signal exiting the medium into detected counts. This information was then used to add shot noise to the simulated DTOFs. The simulator consisted of an external framework written in Matlab with 4 iterators allowing the change of different parameters in a range (e.g. background optical properties, absorption perturbation, features of the IRF etc.) and a central kernel is written in C for computational efficiency, performing the calculus of the homogeneous and perturbed DTOF.

2.3 Figures of merit

Contrast and CNR which are standardized figures of merit defined in the nEUROPt protocol [11] to assess the sensitivity to localized perturbation in both measurements and simulations for an Instrument. They were calculated for sections of the DTOF curve (software gate = 500 ps for both measurements and simulations) by the 'time-windowing' of the curve. This was done for various delays of the rising edge of the gate, with respect to the IRF peak and was noted as t_g.

The contrast is defined as the absolute difference between the unperturbed (i.e. homogeneous medium) and perturbed counts. It was computed for all depths of the inclusions following Eq. 1 [11]:

$$C(t_g) = \frac{N_0(t_g) - N(t_g)}{N_0(t_g)} \quad (1)$$

Where N_0 and N are the total number of counts in a software gate in the unperturbed and perturbed cases respectively. For the measurements, the acquisition of the homogeneous case was performed by moving the perturbation to a depth of 4 cm where its effect was completely negligible.

The CNR was computed following the definition is given in [11] and reported in Eq. 2:

$$CNR(t_g) = \frac{N_0(t_g) - N(t_g)}{\sigma(N_0(t_g))} \quad (2)$$

Where the difference at the numerator was taken over the repetitions of the acquisitions (5 for measurements) for the software gate under consideration, while $\sigma(N_0(t_g))$ is taken as the standard deviation of the number of counts in the homogeneous case for measurements, while for the simulation it is taken as the square root of the homogenous counts.

3. DISCUSSION

The study consists of two parts. First, a comparative study between contrast calculated from experimentally obtained data and those obtained from the simulations. In a second part, we extend the simulation to study the effects of the above mentioned parameters (system, geometrical and optical parameters and measurement strategies) on the contrast and CNR to establish the system/geometrical and optical parameters that have maximum effect on contrast and CNR, thus providing a guideline that allows the scientists to choose the most suitable measurement strategy to obtain the best figures of merit, under the limitations imposed by experimental parameters.

All the parameters affecting the system performance can be classified into three categories, namely i) system parameters, which includes the IRF, average laser power, system responsivity and noise sources (dark counts and afterpulsing), ii) geometrical and optical parameters such as size and depth of perturbation, the background optical

properties of the medium (μ_a and μ'_s) and iii) measurement strategies namely source-detector separation, acquisition time and gate opening delay. The IRF in itself is defined by the following parameters, i) the Full-Width at Half-Maximum (FWHM), ii) the diffusion tail (time constants of a few tens of ps) and iii) a slowly decaying noise tail known as the 'memory effect'[15][10] which sets the limitation on the maximum achievable dynamic range of the system.

For the sake of brevity, we discuss here two cases that describe well the general trends in TD measurements.

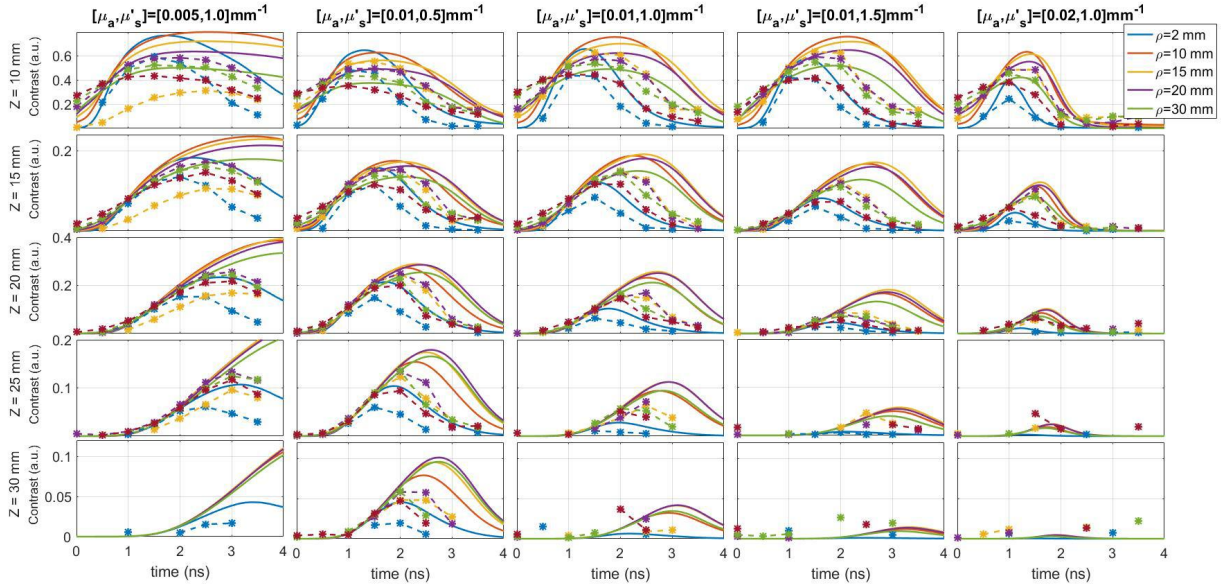

Figure 2. Plot of Contrast vs time (colors represent source-detector distances), with a change in depth of inclusion (z) along the rows and optical properties (μ_a, μ_s') of the medium along the columns, the dashed curves correspond to the measurements and continuous curves correspond to simulated values.

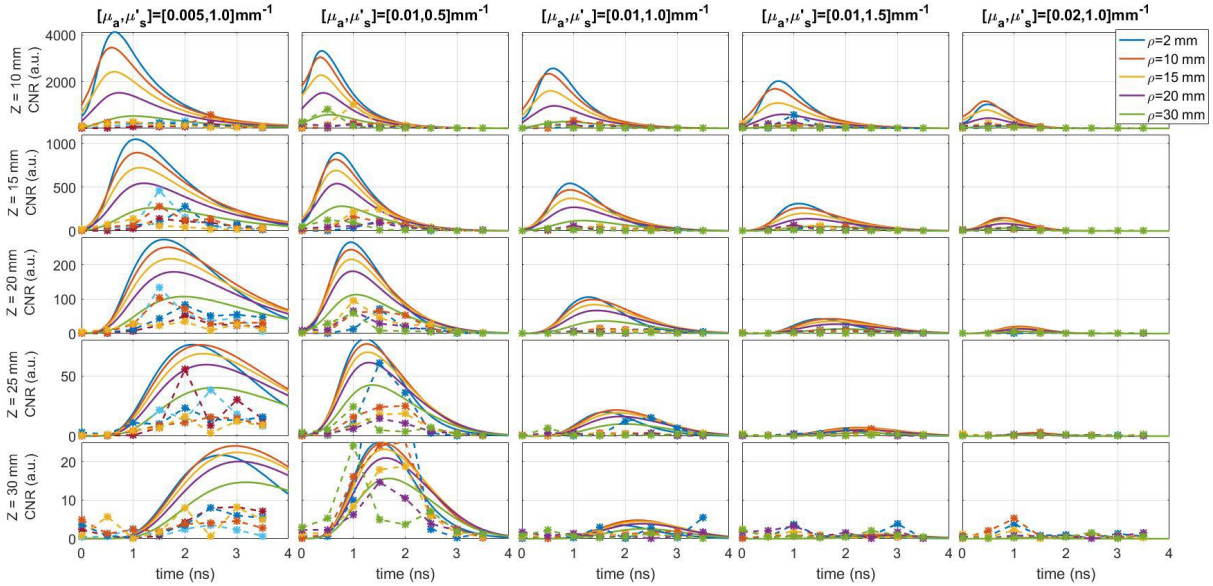

Figure 3. Plot of CNR vs time (colors represent source-detector distances), with change in depth of inclusion (z) along the rows and optical properties (μ_a, μ_s') of the medium along the columns. The dashed curves correspond to the measurements and continuous curves correspond to simulated values.

Figure 2 reports plots of contrast vs time, at different source-detector separations (ρ), depths of inclusion (z) and different values of background absorption (μ_a) and reduced background scattering (μ'_s) of the medium are taken into account in rows and columns respectively. Here we compare the contrast and CNR obtained from measurements (dashed curves) and simulations (continuous curves). There is a fair agreement between measurements and simulations in the case of contrast. In the case of CNR however, as expected the agreement is less so as simulation does not take into account all the noise sources such as fast random fluctuations in laser power. It can be noticed that the change in contrast upon increasing μ_s' is strongly dependent on the depth of inclusion. For superficial inclusions, we see that contrast increases with increasing μ_s', this is because of the number of photons scattered in the direction of the detector increases. However, as the inclusion is placed deeper in the medium, scattering of the medium starts to limit the number of photons reaching the inclusion itself hence, reducing the overall contrast. This can also be seen in the variation of CNR in Figure 3. As per the variation of contrast with μ_a, we see that the contrast decreases at longer times for high μ_a values. The CNR reduces drastically with increase in μ_a as well, implying a reduction in the number of detected photons. For deeper inclusions, the contrast is lower due to the spreading of the sensitivity profile of photons. Additionally, the peak corresponding to maximum contrast shifts towards longer time. This is due to the fact that re-emission time of photons encodes the mean probed depth. Thus, for superficial inclusions, the maximum contrast is provided by photons re-emitter earlier in time compared to those for the deeper inclusions. Crucially, we also observe that the maximum contrast is no longer obtained for small ρ values but for intermediate values (ρ=10-15mm), this can be ascribed to the fact that memory tail limits the dynamic range of the system and hence clamping down the contrast at late times. However, since memory is a signal-dependent phenomenon, the reduction, in contrast, is maximum for small ρ values.

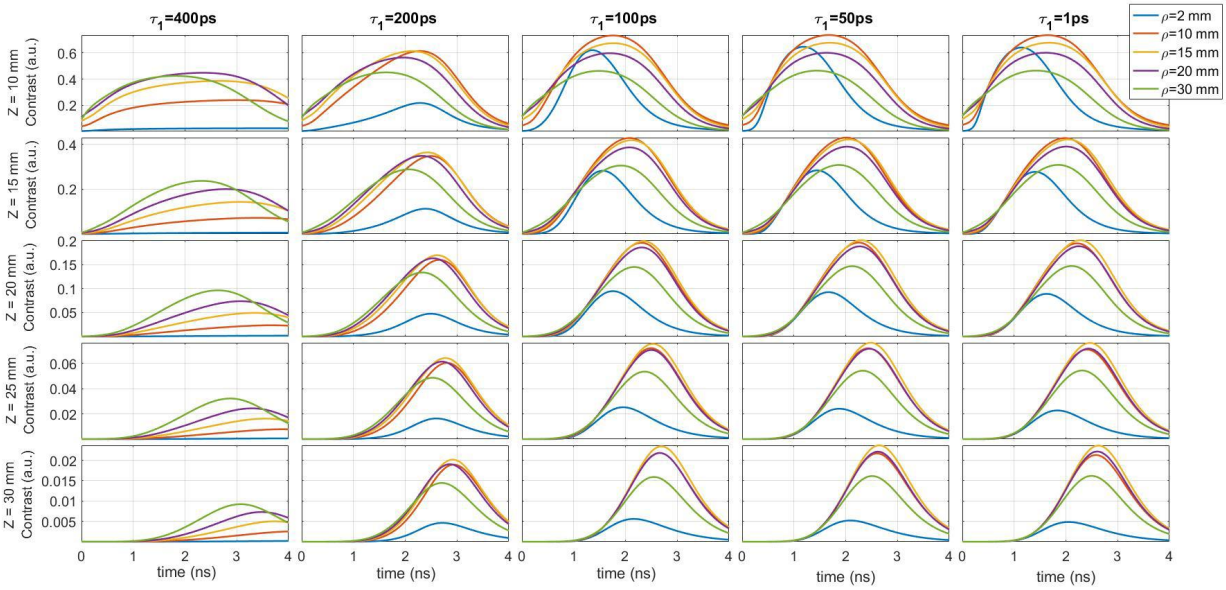

Figure 4. Plot of Contrast vs time, with change in depth of inclusion (z) along the rows and diffusion tail slope (τ_1) along the columns

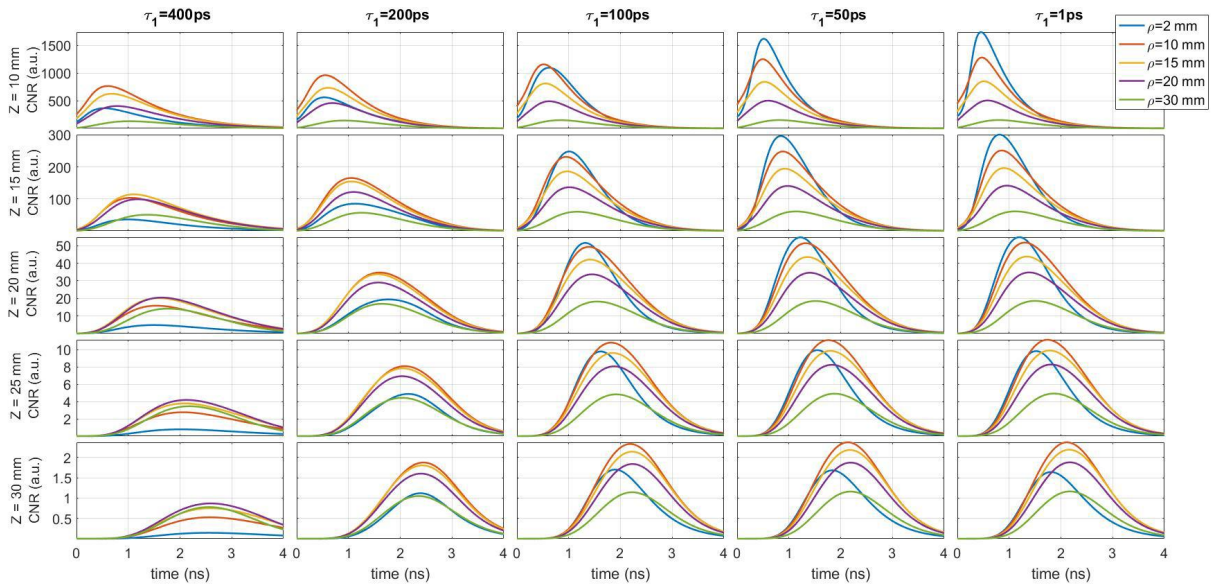

Figure 5. Plot of CNR vs time, with change in depth of inclusion (z) along the rows and diffusion tail slope (τ1) along the columns

Figure 4 and Figure 5 show the contrast vs time and CNR vs time for different source-detector separations. Here we observe the variation in contrast with z and diffusion tail slope (τ_1). As the diffusion tail slope increases, we observe a broadening of the contrast curves as well as a decrease in the absolute value of contrast. However, the decrease, in contrast, is fastest for small ρ as compared to the larger ones. Indeed, for shorter source-detector distances, the reflectance curve is less broadened and so, in the convolution process, a large diffusion tail can dominate with respect to the ideal (i.e. IRF equal to a delta Dirac) response of the medium. In general, the broadening of the contrast curves is due to the fact that there is a leakage of early photons in a temporal region of the curve where the only contribution of late photons are expected[16] . Hence, a longer diffusion tail leads to a broadening of the contrast curve due to the temporal spreading of photons. CNR follows a similar trend.

In conclusion, this study essentially demonstrates that under the influence of the slow tails in the IRF, the use of a small SDS no longer corresponds to optimal contrast and CNR. Furthermore, the optimal SDS lies in the range of 10 to 15 mm. Better design and fabrication can reduce the effect of slow tails in the IRF, but until such time the slow tail sets the main limitation on the dynamic range of time-gated measurements and so to the performances of TDDO systems working with short SDS. This work sets the ground for future studies with next-generation of TDDO components, presently under development, providing useful hints on relevant features that must be taken care of when designing TDDO components. Indeed, as already pointed out in reference [A. Pifferi, D. Contini, A. D. Mora, A. Farina, L. Spinelli, and A. Torricelli, "New frontiers in time-domain diffuse optics, a review," J. Biomed. Opt., vol. 21, no. 9, p. 91310, 2016.], new technological advancements have been recently introduced in the TD diffuse optics (e.g. large area detector, miniaturized laser etc [17][18]) and a new dawn for the TD-instruments can be foreseen. Additionally, this work provides an insight into the interdependency of the parameters and their overall impact on the system performance thus helping the scientists in the design of the new generation of system and on the best experimental conditions to operate the existing system

Acknowledgments: The research leading to these results has received partial funding from the European Union's Horizon 2020 programme under Grant Agreement no. 675332 (BITMAP), and from European Union's Horizon 2020 research and innovation programme under Grant Agreement no. 731877 (SOLUS: Smart OpticaL and UltraSound diagnostics of breast cancer) and under Grant Agreement no. 654148 (Laserlab-Europe). SOLUS is an initiative of the Photonics Public Private Partnership.

REFERENCES

[1] A. Yodh and B. Chance, "Spectroscopy and imaging with diffusing light," *Phys. Today*, vol. 48, no. 3, pp. 34–41, 1995.

[2] T. Durduran, R. Choe, W. B. Baker, and A. G. Yodh, "Diffuse optics for tissue monitoring and tomography," *Reports Prog. Phys.*, vol. 73, no. 7, p. 76701, Jul. 2010.

[3] H. Wabnitz *et al.*, "Time-domain diffuse optical imaging of tissue by non-contact scanning," *Springer Ser. Chem. Phys.*, vol. 111, pp. 561–585, 2015.

[4] G. Quarto *et al.*, "Estimate of tissue composition in malignant and benign breast lesions by time-domain optical mammography," *Biomed. Opt. Express*, vol. 5, no. 10, pp. 3684–98, 2014.

[5] L. Di Sieno *et al.*, "Time-domain diffuse optical tomography using silicon photomultipliers: feasibility study," *J. Biomed. Opt.*, vol. 21, no. 11, p. 116002, 2016.

[6] A. Pifferi, D. Contini, A. D. Mora, A. Farina, L. Spinelli, and A. Torricelli, "New frontiers in time-domain diffuse optics, a review," *J. Biomed. Opt.*, vol. 21, no. 9, p. 91310, 2016.

[7] A. Puszka *et al.*, "Spatial resolution in depth for time-resolved diffuse optical tomography using short source-detector separations," *Biomed. Opt. Express*, vol. 6, no. 1, p. 1, 2015.

[8] E. Alerstam *et al.*, "Single-fiber diffuse optical time-of-flight spectroscopy," *Opt. Lett.*, vol. 37, no. 14, p. 2877, 2012.

[9] H. Wabnitz *et al.*, "Performance assessment of time-domain optical brain imagers, part 1: basic instrumental performance protocol," *J. Biomed. Opt.*, vol. 19, no. 8, p. 86010, 2014.

[10] A. D. Mora *et al.*, "Memory effect in silicon time-gated single-photon avalanche diodes," *J. Appl. Phys.*, vol. 117, no. 11, 2015.

[11] H. Wabnitz *et al.*, "Performance assessment of time-domain optical brain imagers, part 2: nEUROPt protocol," *J. Biomed. Opt.*, vol. 19, no. 8, p. 86012, 2014.

[12] S. J. Madsen, M. S. Patterson, and B. C. Wilson, "The use of India ink as an optical absorber in tissue-simulating phantoms," *Phys. Med. Biol.*, vol. 37, no. 4, pp. 985–993, 1992.

[13] F. Martelli *et al.*, "Phantoms for diffuse optical imaging based on totally absorbing objects, part 2: experimental implementation," *J. Biomed. Opt.*, vol. 19, no. 7, p. 76011, 2014.

[14] A. Sassaroli *et al.*, "Forward solvers for photon migration in the presence of highly and totally absorbing objects embedded inside diffusive media," *J. Opt. Soc. Am. A*, vol. 31, no. 3, p. 460, 2014.

[15] A. Dalla Mora, D. Contini, A. Pifferi, R. Cubeddu, A. Tosi, and F. Zappa, "Afterpulse-like noise limits dynamic range in time-gated applications of thin-junction silicon single-photon avalanche diode," *Appl. Phys. Lett.*, vol. 100, no. 24, 2012.

[16] D. Contini *et al.*, "Effects of time-gated detection in diffuse optical imaging at short source-detector separation," *J. Phys. D. Appl. Phys.*, vol. 48, no. 4, 2015.

[17] E. Martinenghi, L. Di Sieno, D. Contini, M. Sanzaro, A. Pifferi, and A. Dalla Mora, "Time-resolved single-photon detection module based on silicon photomultiplier: A novel building block for time-correlated measurement systems," *Rev. Sci. Instrum.*, vol. 87, no. 7, 2016.

[18] L. Di Sieno *et al.*, "Miniaturized pulsed laser source for time-domain diffuse optics routes to wearable devices," *J. Biomed. Opt.*, vol. 22, no. 8, p. 1, 2017.

*Anurag.behera@polimi.it; phone 39 3662315626